J. Phys.: Condens. Matter **20** (2008) 354002 (7pp) doi:10.1088/0953-8984/20/35/354002

Effect of tip flexibility on stick–slip motion in friction force microscopy experiments

Z Tshiprut[1], A E Filippov[2] and M Urbakh[1]

[1] School of Chemistry, Tel Aviv University, 69978 Tel Aviv, Israel
[2] Donetsk Institute for Physics and Engineering of NASU, 83144, Donetsk, Ukraine

E-mail: urbakh@post.tau.ac.il

Received 31 January 2008, in final form 4 March 2008
Published 11 August 2008
Online at stacks.iop.org/JPhysCM/20/354002

Abstract

We have investigated the effect of tip flexibility on stick–slip dynamics, treating the motion of the tip apex and the cantilever within a Langevin description. We have found that the dynamical system, which includes the cantilever and the tip apex, exhibits a rich variety of regimes of motion depending on the values of the dissipation constants associated with the translational motion of the apex and the bending motion of the tip. The proposed model explains the fine structure of the stick–slip patterns and the wide variation of slip durations, between microseconds and milliseconds, observed in recent experiments with a friction force microscope (Maier *et al* 2005 *Phys. Rev.* B **72** 245418). The results of our full Langevin description are compared with the predictions of the single-spring Prandtl–Tomlinson model and the hybrid Langevin–Monte Carlo approach, which has recently been proposed.

(Some figures in this article are in colour only in the electronic version)

1. Introduction

It has been recognized recently [1–8] that the flexibility of a friction force microscope (FFM) tip may strongly influence the dynamics of stick–slip processes observed in atomic scale friction experiments. The torsional elasticity of a typical silicon cantilever used for atomic friction measurements is $K = 62$ N m^{-1} [1]. However, the effective spring constant, $K_{\rm eff}$, which is estimated in experiments from the slope of the sticking part of the force traces, is usually much smaller than the stiffness of the cantilever, $K_{\rm eff} \approx 1$–3 N m^{-1}. The effective spring constant can be presented as the result of two coupled springs in series, which are associated with the elastic deformation of cantilever, K, and tip apex, k, according to $K_{\rm eff}^{-1} = K^{-1} + k^{-1}$. Then for the values $K = 62$ N m^{-1} and $K_{\rm eff} = 3.7$ N m^{-1} taken from the experiment in [1], it follows that $k = 3.5$ N m^{-1} and the tip apex is much softer than the rest of the cantilever. It was found [1, 7] that this is true for most cantilevers, irrespective of the material or shape of the tip.

Traditionally, FFM is described by a single-spring Prandtl–Tomlinson model [3, 4, 9–11], in which an effective mass, close to that of the cantilever, is pulled along the surface by an effective spring $K_{\rm eff}$, which accounts for the flexibility of both the cantilever and the tip. For a long time it was assumed that the flexibility of the tip does not give rise to new dynamical phenomena which are not described by the traditional Prandtl–Tomlinson model. First experimental and theoretical indications for nontrivial effects of the tip flexibility have appeared only recently [1–7]. They include observation of a wide variation of slip durations up to several milliseconds [1], a suggestion of an additional channel of dissipation that may result in a nonmonotonous velocity dependence of friction [3, 4], and predictions of new regimes of motion where the tip apex can be partially or completely delocalized [5–7].

In a series of recent publications [5–7] the effect of bending motion of the FFM tip, which is associated with fast movements of the tip apex with ultra-low effective mass, on the observable friction phenomena has been systematically studied. The calculations have been performed within a hybrid numerical scheme that combines a Langevin description of the cantilever motion with a Monte Carlo treatment of the thermally activated jumps of the tip apex. The authors of [5–7] used a simple approximation for the jump rate and neglected dissipative forces resulting from the motion of the apex with respect to the surface and from the tip deformation. They found that: (i) the motion of the cantilever measured in FFM experiments can be very different from the rapid motion of the tip apex which is probing the surface; (ii) the influence of thermal effects on friction can be much stronger than

that expected from the traditional single-spring–single-mass description.

In this paper we study the effect of the tip flexibility on the dynamics of friction, treating the motion of the tip apex and the cantilever together with the rest of the tip on an equal footing, within a full Langevin description. Contrary to the previous works [5–7], we focus on the influence of channels of energy dissipation associated with the apex translational motion and the tip bending on the observable regimes of the frictional response. A variation of the mean friction force with the scanning velocity has been calculated, and it shows a strong dependence on the dissipation constants and on the stiffness of the cantilever. The proposed description explains a fine structure of the stick–slip patterns and a wide variation of slip durations up to several milliseconds observed in recent FFM experiments [1]. A comparison of the results of the full Langevin description with the prediction of the single-spring Prandtl–Tomlinson approximation [3, 4] has revealed a range of applicability of the latter model.

2. The model

In order to study the effect of the tip flexibility on the dynamics of friction, we consider a two-mass–two-spring model (see figure 1), with one mass, m, associated with the bending motion of the tip (the effective mass of the tip apex) and the other mass, M, accounting for the combined inertia of the cantilever and the rest of the tip. Then the dynamical behaviour of the system (cantilever + tip apex) is governed by the coupled Langevin equations:

$$M\ddot{X}(t) + \Gamma\dot{X} + \eta_c(\dot{X} - \dot{x}) + k(X - x) + K(X - Vt) = f_X \quad (1)$$

$$m\ddot{x} + \eta_c(\dot{x} - \dot{X}) + \eta_s\dot{x} + k(x - X) + \partial U(x)/\partial x = f_x. \quad (2)$$

Here the first equation describes the motion of the cantilever, whose position is given by the coordinate X, and the second one describes the motion of the tip apex with a coordinate x. The cantilever is pulled by a spring of spring constant K connected to a support which moves with a constant velocity V, and the cantilever is elastically coupled to the apex through the spring with stiffness k. The apex–surface interaction is described by the periodic potential $U(x) = U_0\cos(\frac{2\pi}{a}x)$, where a is its periodicity, and U_0 is the amplitude of the potential corrugation. The parameters Γ, η_s and η_c are responsible for the dissipation of the kinetic energy due to the lateral motion of the cantilever and the apex, and due to deformation of the tip, respectively. The effect of thermal fluctuations on the motion of the cantilever and the apex is given by independent random forces, $f_X(t)$ and $f_x(t)$, which are δ-correlated, $\langle f_X(t)f_X(t')\rangle = 2(\Gamma + \eta_c)k_BT\delta(t - t')$ and $\langle f_x(t)f_x(t')\rangle = 2(\eta_s + \eta_c)k_BT\delta(t - t')$.

Within a quasistatic description of the cantilever motion, for which $k(X - x) + K(X - Vt) = 0$, the two coupled equations (1) and (2) reduce to a single dynamical equation for the apex

$$m\ddot{x} + \eta_c(\dot{x} - V)(K_{\rm eff}/k) + \eta_s\dot{x} + K_{\rm eff}(x - Vt) + \partial U(x)/\partial x = f_x, \quad (3)$$

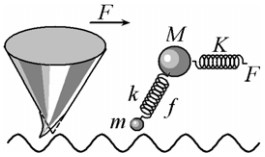

Figure 1. Sketch of the geometry of the two-spring–two-mass model of a friction force microscope.

where $K_{\rm eff} = Kk/(K + k)$ and the experimentally measured lateral force reads as

$$F = K(X - Vt) = K_{\rm eff}(x - Vt). \quad (4)$$

Except for the coefficient $(K_{\rm eff}/k)$ which is close to unity for $K \gg k$, equation (3) coincides with that suggested previously in [3, 4]. One of the objectives of this study is to understand under what conditions the reduced description (3) captures the main features of the frictional response predicted by the full Langevin description in (1) and (2).

3. Results and discussion

Depending on the choice of parameters, the dynamical system described by equations (1) and (2) exhibits a rich variety of regimes of motion. The results presented below have been obtained for the parameters $M = 5.5\times10^{-11}$ kg, $k = 3$ N m^{-1} and $a = 0.66$ nm which were taken from the experiments of [1]. Both stiff and soft cantilevers with $K = 62$ and 6 N m^{-1}, which are used in experiments [1, 12], have been considered. We have chosen a value of potential corrugation $U_0 = 0.38$ eV for which the simulations produce stick–slip patterns similar to the experimental results [1]. For this value of corrugation, the Tomlinson parameter $\gamma = \frac{(2\pi)^2U_0}{ka^2} = 1.8$. So far not much is known about the values of dissipation constants, Γ, η_s and η_c and therefore in order to understand the effect of these parameters on dynamics we have performed simulations in a wide range of the parameters 10^{-4} kg s^{-1} $<$ Γ, η_s, η_c $<$ 10^{-10} kg s^{-1}. Recent studies suggested very different estimations for the effective mass of the tip apex ranging from $m = (10^{-9}$–$10^{-12})M$ [5–7] to $m = M/10$ [1, 3]. Most of the results presented below have been obtained for the case of overdamped motion of the apex (neglecting the inertia term in equation (2)) that is typical for nanoscale systems. Moreover, we have found that the frictional response is almost independent of the apex mass m within the range $0 < m < m_{\rm max}$, where $m_{\rm max} = 10^{-1}(\eta_s + \eta_c)^2/[(2\pi)^2U_0/a^2]$. These conditions correspond to an overdamped dynamics of apex. For the values of parameters used in the calculations presented below, $\eta_s + \eta_c \approx 10^{-5}$ kg s^{-1}, 10^{-7} kg s^{-1} and 10^{-9} kg s^{-1}, the threshold mass $m_{\rm max}$ is of the order of $10^{-1}M$, $10^{-5}M$ and $10^{-9}M$, respectively.

Our calculations show that the shape of stick–slip patterns for the cantilever motion predicted by equations (1) and (2) is dictated by the values of the parameters η_s and η_c which are responsible for the energy dissipation to the excitations in the substrate and in the tip. The dissipation constant Γ mostly

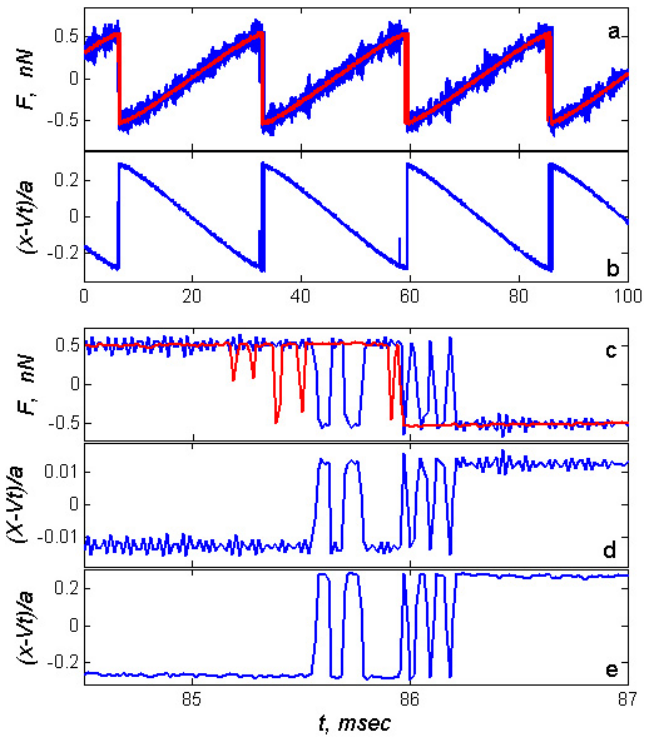

Figure 2. Lateral force ((a), (c)) and relative apex ((b), (e)) and cantilever (d) positions versus time calculated for a stiff cantilever, $K = 62$ N m^{-1}, with a sampling frequency of 3.3 MHz. Black and gray (blue and red online) curves show results of the full Langevin calculations in equations (1) and (2) and of the quasistatic approximation in equation (3), respectively. The panels (c)–(e) display an enlarged view of the slip region. Parameter values: $M = 5.5 \times 10^{-11}$ kg, $k = 3$ N m^{-1}, $a = 0.66$ nm, $U_0 = 0.38$ eV, $V = 25$ nm s^{-1}, $\eta_s = \eta_c = \Gamma = 10^{-7}$ kg s^{-1}.

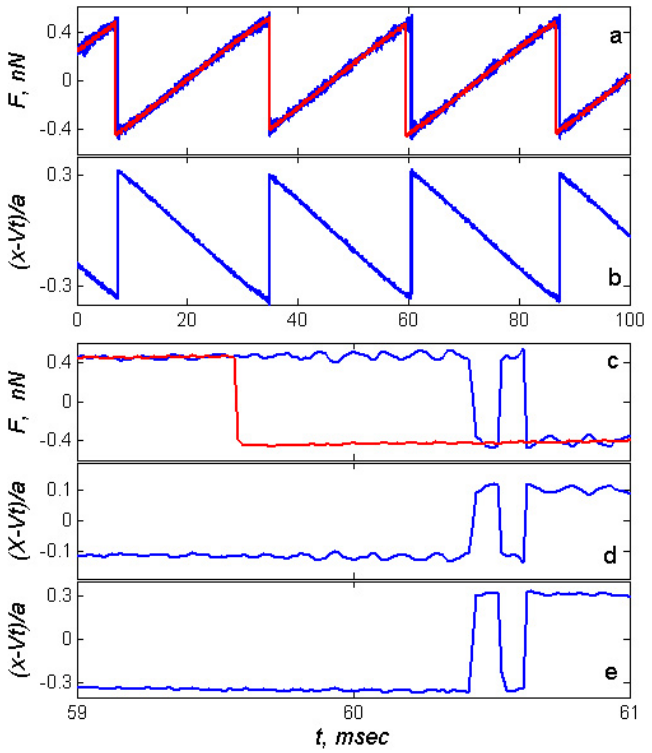

Figure 3. Lateral force ((a), (c)) and relative apex ((b), (e)) and cantilever (d) positions versus time calculated for a soft cantilever with $K = 6$ N m^{-1}. Black and gray (blue and red online) curves show results of the full Langevin calculations in equations (1) and (2) and of the quasistatic approximation in equation (3), respectively. The panels (c)–(e) display an enlarged view of the slip region. Parameters as in figure 2.

controls damping of mechanical oscillations with a frequency $\nu_c = \sqrt{K/M}$.

For $\eta_s \geqslant 10^{-5}$ kg s^{-1}, irrespective of the values of other dissipation constants, the cantilever exhibits a traditional stick–slip motion. Here each slip of the apex to the next accessible well of the substrate potential is followed by a corresponding slip of the cantilever. Then for low scanning velocities where a stick–slip motion is observed, the results of the reduced description (3) are in excellent agreement with the direct solutions of the coupled equations (1) and (2). However, it should be noted that in the range of higher scanning velocities corresponding to a 'smooth' sliding the calculations with equation (3) may differ from those obtained with equations (1) and (2). This disagreement results from the effects of an additional channel of dissipation, $\Gamma\dot{X}$, and mechanical oscillations at the characteristic frequency, ν_c, which appear in the full description (1) and (2) but are not included in the reduced model (3). We discuss these effects below.

The frictional response becomes more complex for lower values of the dissipation constant, $\eta_s \leqslant 10^{-6}$ kg s^{-1}. Figures 2 and 3 show that in this case the stick–slip events are accompanied by thermally activated jumps of the apex between the two accessible wells of the combined potential, $U_{\text{apex}}(x, X) = U(x) + k(x - X)^2/2$ (see inset to figure 4). These jumps occur when the cantilever comes close to the maximum of the potential corrugation ($X \approx an, n = 0, \pm1, \pm2\ldots$) and the lateral force, F, approaches its maximum value. Otherwise the apex is located within one well only. For a given value of η_s the rate of the apex jumps decreases with η_c. The jumps of the apex manifest themselves in the corresponding oscillations of the measured lateral force (see figures 2 and 3). As a result, the experimentally observed slip time becomes significantly longer than that predicted by a traditional, one-spring Tomlinson model. Our calculations show that the effect of tip flexibility extends the slip times from the microsecond or tenths of microsecond scale to milliseconds, as was observed experimentally [1].

Figure 2 demonstrates that in this case the displacement of the cantilever follows the apex jumps but for the stiff cantilever ($K = 62$ N m^{-1}) the amplitude of the cantilever oscillations is significantly smaller (by one or two orders of magnitude) than that of the apex (see panels (d) and (e)). It should be noted that even in the absence of the multiple jumps of the apex (for $\eta_s \geqslant 10^{-5}$ kg s^{-1}) the cantilever closely follows the motion of the stage, $X \approx Vt$, exhibiting very short slips with the length, which is of the order of $(10^{-1}$–$10^{-2})a$, where a is the period of the surface potential $U(x)$. This is the apex that performs slips with the length of the order of a.

Owing to the almost steady motion of the cantilever, the quasistatic approximation (3) provides a reasonable description of friction for the stiff cantilever with $K = 62$ N m^{-1} in a

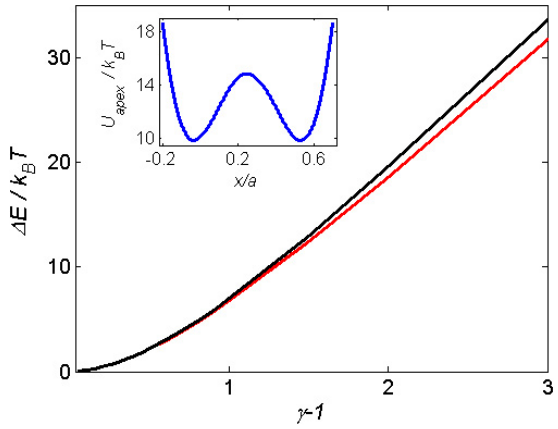

Figure 4. Height of the barrier which separates two accessible wells of the potential experienced by the apex as a function of the Tomlinson parameter γ. Black and gray (black and red online) curves show the results given by numerical calculations and by the analytical equation (6), respectively. Calculations have been done for the cantilever located close to the maximum of the potential corrugation. The potential experienced by the apex is shown in the inset. Parameter values: $U_0 = 0.38$ eV, $a = 0.66$ nm, $k = 3$ N m^{-1}.

wide range of the parameters, η_s, η_c, and Γ. However, our calculations show that it may be inaccurate even in this case. For instance, we found that for $\eta_s = 10^{-7}$ kg s^{-1} and $\eta_c = 10^{-5}$ kg s^{-1}, the full model predicts multiple jumps of the apex, while the quasistatic approximation does not reproduce this effect. As is shown below, this disagreement can be explained by the effect of correlated motion of the apex and the cantilever on the probability of the thermally activated jumps which is not included in the quasistatic model.

A disagreement between the results of the quasistatic approximation and the full description becomes more substantial in the case of a soft cantilever. The slip length of the cantilever increases with a decrease of its stiffness, K, and for a soft cantilever with $K = 6$ [12] it is only twice as small as the apex slip length. In this case one may expect significant deviations of the results of the quasistatic approximation from the full description (1) and (2).

In order to estimate a rate of apex jumps, $r_{\rightarrow,\leftarrow}$, between the two accessible wells of the potential $U_{\rm apex}(x, X)$ we use the Kramer's equation [13]

$$r_{\rightarrow,\leftarrow}(X) = \frac{\omega_{l,r}(X)\omega_{\max}(X)}{2\pi m \eta_{\rm eff}} \exp[-\Delta E_{\rightarrow,\leftarrow}(X)/k_{\rm B}T]. \quad (5)$$

Here $\Delta E_{\rightarrow}(X)$ and $\Delta E_{\leftarrow}(X)$ are the instantaneous barrier heights for the jumps from the left well to the right one and back, which depend on the cantilever position X, $\omega_{l,r,\max}(X) = \sqrt{m|\partial^2 U_{\rm apex}(x, X)/\partial x^2||_{x=x_{l,r,\max}}}$ are the frequencies of small oscillations at the minima of the left and right potential wells, $x = x_{l,r}$, and at the maximum of the potential, $x = x_{\max}$, respectively, and $\eta_{\rm eff}$ is the effective dissipation constant that determines a rate of energy dissipation to the substrate and tip. The latter quantity can be estimated as $\eta_{\rm eff} = (\eta_s + \delta\eta_c)$, where a coefficient $\delta < 1$ was introduced in order to take into account that correlated oscillations of the apex and tip reduce the rate of energy dissipation to the tip.

The probability of thermally activated jumps of the apex becomes maximal when the cantilever approaches the maximum of the surface potential $U(x)$. Then the height of the barrier, $\Delta E = \Delta E_{\rightarrow}(X) = \Delta E_{\leftarrow}(X)$, which separates the two wells, and the frequencies $\omega_{l,r,\max}$ can be estimated by expanding the potential $U_{\rm apex}(x, X)$ in the vicinity of its maximum at $x = an$. As a result we get the following expression for ΔE and $\omega_{l,r}\omega_{\max}$

$$\Delta E = 1.5U_0 \left(\frac{\gamma - 1}{\gamma}\right)^2 \left(1 + 0.2\frac{\gamma - 1}{\gamma}\right) \quad (6)$$

$$\omega_{l,r}\omega_{\max} = \sqrt{2}k(\gamma - 1) \quad (7)$$

where $\gamma = \frac{(2\pi)^2 U_0}{ka^2}$ is the Tomlinson parameter. Figure 4 shows that equation (6) closely approximates the result of numerical calculations of the height of the barrier in a wide range of parameters U_0 or γ. It should be noted that for γ close to unity the height of the potential barrier, ΔE, is considerably lower than U_0. In particular, for $U_0 = 0.38$ eV, $k = 3$ N m^{-1} and $a = 0.66$ nm the Tomlinson parameter $\gamma = 1.8$, $\Delta E = 0.125$ eV, and equation (5) give the following estimation for the rate of apex jumps

$$r_{\rightarrow,\leftarrow} = \frac{3.4 \times 10^{-3}\ \text{kg s}^{-2}}{\eta_{\rm eff}}. \quad (8)$$

The above equation shows that for the dissipation constants, 10^{-8} kg s$^{-1} \leqslant \eta_s, \eta_c < 10^{-6}$ kg s^{-1} the rate of apex jumps is considerably higher than the washboard frequency, V/a, which for $V = 25$ nm s^{-1} equals 40 s^{-1}, but $r_{\rightarrow,\leftarrow}$ is still smaller or of the same order as the characteristic frequency of the cantilever, $\nu_c \approx 10^6$ s^{-1}. As a result in this range of parameters the tip apex performs several thermally activated jumps back and forth between the accessible wells of the potential $U_{\rm apex}$ during one stick–slip event, and the cantilever follows the jumps of the apex (see figures 2 and 3). The average number of jumps per one stick–slip interval is reduced with a decrease of the cantilever stiffness, K, since for low values of K the amplitude of the cantilever oscillations increases and it spends less time close to the potential maximum where the jump rate is maximal (see figure 3).

The probability distribution function (PDF) for the time-averaged position of the apex with respect to the cantilever, $x - X$, is presented in figure 5. The two maxima in the PDF manifest the presence of the two accessible wells in the potential experienced by the apex. Figure 5 shows that the PDF which has been obtained from the simulations of the nonequilibrium Langevin dynamics is well described by the equilibrium distribution function $P(x - X) \propto \int dt \exp[-U_{\rm apex}(x(t), X(t))]$. With increase of scanning velocity or/and the dissipation constants η_s, η_c the nonequilibrium PDF becomes asymmetric, with a left maximum higher than the right one, which reflects a lag of the apex behind the cantilever. Under these conditions ($V > 250$ nm s^{-1}) a difference between the nonequilibrium and equilibrium PDFs becomes considerable.

It should be noted that equation (5) can be also applied to estimate the rate of jumps in the quasistatic model. In this case

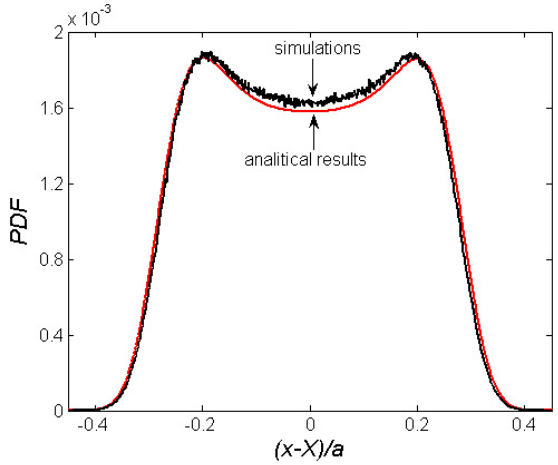

Figure 5. Probability distribution function for the time-averaged position of the apex with respect to the cantilever. The black curve shows results of Langevin simulations and the gray (red online) curve presents the equilibrium distribution function. Parameters as in figure 2.

$\delta = 1$ and X should be substituted by Vt. Our calculations show that the quasistatic description may underestimate the probability of the apex jumps, because it does not include a correlated motion of the apex and the cantilever, and in this way undervalues the apex diffusion. For instance, for $\eta_s = 10^{-7}$ kg s^{-1} and $\eta_c < 10^{-5}$ kg s^{-1} the full description shows multiple jumps of the apex and the cantilever, but the quasistatic description predicts usual, structureless stick–slip motion without multiple jumps.

In the Monte Carlo simulations of the apex jumps performed in [5–7] the jump rate has been described by an equation which is similar to equation (5) but with the preexponential factor given by the frequency of the apex bending vibrations $\nu_{apex} = \sqrt{k/m}$. For the parameters used in [5–7], $m = 10^{-20}$ kg and $k = 3$ N m^{-1}, this frequency equals $\nu_{apex} = 1.7 \times 10^{10}$ s^{-1}. Comparing this value with the preexponential factor in equation (5) we see that in order to get a rate of apex jumps which is comparable with that assumed in [5–7] the dissipation constant η_{eff} should be of the order of 10^{-10}–10^{-11} kg s^{-1}. Figure 6 demonstrates that already for $\eta_s = \eta_c = 10^{-9}$ kg s^{-1} the apex performs rapid jumps with the rate which is higher than the characteristic frequency of the cantilever, ν_c, and the cantilever cannot follow the apex jumps. In this case the measured lateral force exhibits a smoothened stochastic stick–slip motion with a slip time lying in the range of 2 ms. This regime of motion has been predicted recently [5–7] and was named 'stuck in slipperiness'.

The stick–slip patterns, which are similar to those presented in figures 2, 3, and 6, have also been found for lower values of the potential corrugation, U_0 (but still $\gamma > 1$). However, in this case the thermally activated jumps of the apex already occur for higher values of the dissipation constants, η_s and η_c, and slip times become longer than those shown in figures 2, 3, and 6. Thus for $U_0 = 0.24$ eV, which corresponds to the Tomlinson parameter $\gamma = 1.17$, the multiple apex jumps start to show up at $\eta_s, \eta_c \approx 10^{-4}$ kg s^{-1}, and the rapid jump regime of motion (as in figure 6) appears at $\eta_s, \eta_c \approx 10^{-6}$ kg s^{-1}. In the latter regime we observed gradual slips with slip times of the order of 5 ms.

Our calculations show that for the low potential corrugation (for instance, for the Tomlinson parameter $\gamma = 1.17$) the process of slipping may pass through intermediate states as was found experimentally in [1]. The results presented in figure 7 demonstrate that even more than one intermediate state may be observed. For the values of γ which are close to unity, the slipping through the intermediate state has also been found in hybrid Langevin–Monte Carlo simulations [6, 7]. However, it should be noted that for $\gamma = 1.17$ the height of the barrier separating two wells of the potential $U_{apex}(x)$ is smaller than k_BT, i.e. $\Delta E = 0.32k_B$ T. Under these conditions the application of the Monte Carlo description of apex motion with the jump rate given by the transition state theory becomes problematic. We found (see figure 7(b)) that

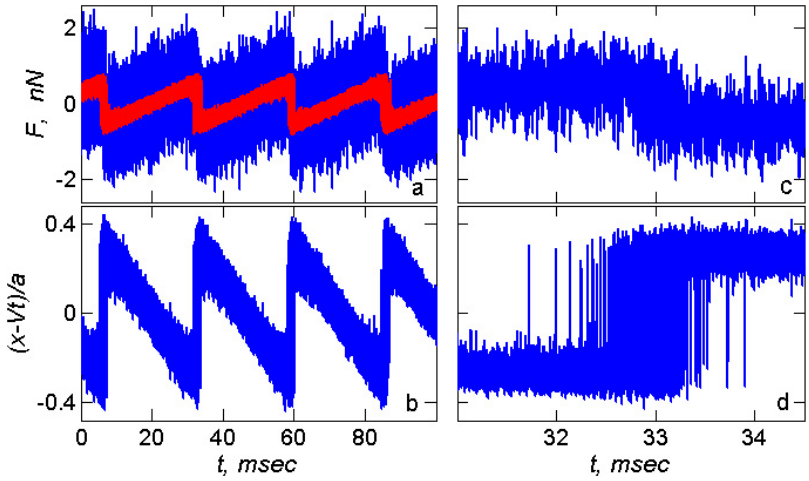

Figure 6. Lateral force ((a), (c)) and relative apex position ((b), (d)) versus time calculated for a stiff cantilever with $K = 62$ N m^{-1}. Black and gray (blue and red online) curves show results of the full Langevin calculations in equations (1) and (2) and of the quasistatic approximation in equation (3), respectively. The panels (c) and (d) display an enlarged view of the slip region. Parameter values: $\eta_s = \eta_c = 10^{-9}$ kg s^{-1}, $\Gamma = 10^{-5}$ kg s^{-1}, other parameters as in figure 2.

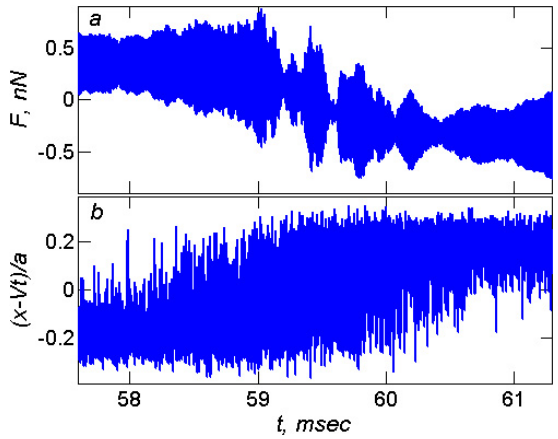

Figure 7. Slipping through intermediate states. An enlarged view of the lateral force (a) and the relative position of the apex (b) in the slip region with a sampling frequency of 3.3 MHz. Parameter values: $U_0 = 0.24$ eV, $\eta_s = \eta_c = \Gamma = 10^{-9}$ kg s^{-1}, other parameters as in figure 2.

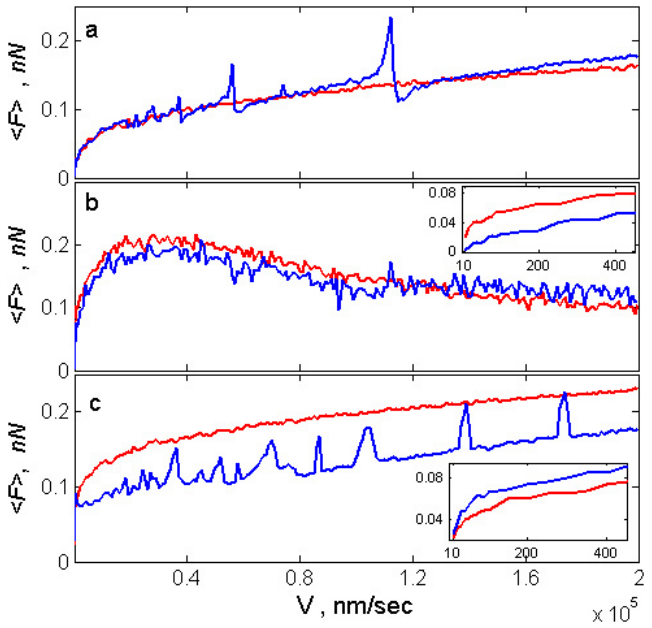

Figure 8. Time-averaged lateral force as a function of scanning velocity. Insets present an enlarged view of the low velocity region. Black and gray (blue and red online) curves show results of the full Langevin calculations in equations (1) and (2) and of the quasistatic approximation in equation (3), respectively. Parameter values: (a) $K = 62$ N m^{-1}, $\eta_s = \eta_c = \Gamma = 10^{-7}$ kg s^{-1}, (b) $K = 62$ N m^{-1}, $\eta_s = \Gamma = 10^{-7}$ kg s^{-1}, $\eta_c = 10^{-5}$ kg s^{-1}, and (c) $K = 6$ N m^{-1}, $\eta_s = \eta_c = \Gamma = 10^{-7}$ kg s^{-1}, other parameters as in figure 2.

when the cantilever approaches the maximum of the surface potential, the tip apex is completely delocalized on the interval $\approx 0.5a$ around the maximum of $U(x)$, rather than performing jumps between two wells of $U_{\text{apex}}(x)$.

Figure 8 presents velocity dependences of the mean lateral force which have been calculated for the stiff and soft cantilevers. Experimental and theoretical studies of velocity dependence of friction have attracted a lot of attention recently [1–4, 11, 14–19], and it has been found that the energy dissipation associated with the tip bending may result in a nonmonotonous variation of friction with the scanning velocity [3, 4]. As has been discussed above, the quasistatic description typically provides a good approximation of the frictional force for the stiff cantilever in the range of low scanning velocities where the stick–slip motion is observed. In this case the deviations from the full description become significant only in the range of parameters (for instance, for $\eta_s = 10^{-7}$ kg s^{-1} and $\eta_c < 10^{-5}$ kg s^{-1}) where the quasistatic description fails to reproduce multiple jumps of the cantilever predicted by equations (1) and (2) (see figure 8(b)). For higher scanning velocities the full calculations predict resonance peaks in the mean lateral force for the washboard frequencies, V/a, which are equal to the characteristic frequency of the cantilever, ν_c, and its multiple harmonics and subharmonics. These resonances are absent in the quasistatic description. It should be noted that the resonances predicted by the full Langevin description are washed out for higher values of the dissipation constants, Γ and η_c. Another source of disagreement at high scanning velocities stems from the influence of an additional channel of dissipation, $\Gamma\dot{X}$, which appears in the full description (1) and (2) but is not included in the quasistatic approximation.

In contrast to the case of the stiff cantilever, for a soft one the mean friction force calculated within the quasistatic approximation deviates significantly from the result of the full Langevin description over the entire interval of velocities considered here (see figure 8(c)). This disagreement results from a considerable departure of the trajectory, $X(t)$, of the soft cantilever from the steady motion Vt. For $K = 6$ N m^{-1} the slip length and the length of the cantilever jumps become of the order of the period a.

Explicitly including the dynamics of the tip apex not only affects the shape of the stick–slip oscillations and the magnitude of the mean friction force but also influences the value of critical velocity, V_c, for a transition from the stick–slip motion to sliding. Thus for the parameter values used in figures 8(a) and (c) the full Langevin description gives $V_c \approx 20$ μm s^{-1} and 10 μm s^{-1}, respectively, while the quasistatic approximation predicts a much higher critical velocity, $V_c \approx 3$ mm s^{-1}, for the corresponding values of parameters. The values of the critical velocities predicted by both models decrease with increase of the dissipation constants η_s, η_c associated with the apex motion, and only slightly depend on Γ.

4. Summary

We have investigated the effect of tip flexibility on the dynamics of the stick–slip motion observed in FFM experiments. Both the motion of the tip apex and the cantilever have been treated within a full Langevin description focusing on the effect of different energy dissipation channels on the frictional response. The dynamical system, which includes the cantilever and the tip apex, exhibits a rich variety of regimes of motion, depending on the values of the dissipation constants associated with the translational motion of the apex

and the bending motion of the tip. The proposed model explains the fine structure of the stick–slip patterns and the wide variation of slip durations between microseconds and milliseconds observed in recent FFM experiments [1]. We have found conditions under which the results of the full Langevin description agree with the predictions of the hybrid Langevin–Monte Carlo approach introduced in [5–7]. A range of applicability of the quasistatic approximation (single-spring Prandtl–Tomlinson model) has been established.

Acknowledgments

The authors are grateful to S Yu Krylov and J W M Frenken for useful discussions. MU acknowledges the support of the Israel Science Foundation (grant No. 1116/05).

References

[1] Maier S, Sang Yi, Filleter T, Grant M, Bennewitz R, Gnecco E and Meyer E 2005 *Phys. Rev.* B **72** 245418
[2] Socoliuc A, Gnecco E, Maier S, Pfeiffer O, Baratoff A, Bennewitz R and Meyer E 2006 *Science* **313** 207
[3] Reimann P and Evstigneev M 2004 *Phys. Rev. Lett.* **93** 230802
[4] Reimann P and Evstigneev M 2005 *New J. Phys.* **7** 25
[5] Krylov S Yu, Dijksman J A, van Loo W A and Frenken J W M 2006 *Phys. Rev. Lett.* **97** 166103
[6] Abel D, Krylov S Yu and Frenken J W M 2007 *Phys. Rev. Lett.* **99** 166102
[7] Krylov S and Frenken J W M 2007 *New J. Phys.* **9** 1367
[8] Luan B Q and Robbins M O 2004 *Phys. Rev. Lett.* **93** 036105
[9] Prandtl L 1928 *Z. Angew. Math. Mech.* **8** 85
[10] Tomlinson G A 1929 *Phil. Mag.* **7** 905
[11] Muser M H, Urbakh M and Robbins M O 2003 *Adv. Chem. Phys.* **126** 187
[12] Dienwiebel M, Verhoeven G S, Pradeep N, Frenken J W M, Heimberg J A and Zandbergen H W 2004 *Phys. Rev. Lett.* **92** 126101
[13] Hanngi P, Talkner P and Borkovec M 1990 *Rev. Mod. Phys.* **62** 251
[14] Sang Y, Dube M and Grant M 2001 *Phys. Rev. Lett.* **87** 174301
[15] Dudko O, Filippov A E, Klafter J and Urbakh M 2002 *Chem. Phys. Lett.* **352** 499
[16] Sills S and Overney R 2003 *Phys. Rev. Lett.* **91** 095501
[17] Urbakh M, Klafter J, Gourdon D and Israelachvili J 2004 *Nature* **430** 525
[18] Krylov S Y, Jinesh K B, Valk H, Dienwiebel M and Frenken J W M 2005 *Phys. Rev.* E **71** 065101
[19] Muser M H 2002 *Phys. Rev. Lett.* **89** 224301